Received: 14 November 2018 | Revised: 22 September 2019 | Accepted: 8 November 2019

DOI: 10.1002/zamm.201800293

EDITOR'S CHOICE

Investigations on amplitude adaptive sequential friction-spring dampers

Jimmy Aramendiz | **Alexander Fidlin** | **Kan Lei**

Institute of Engineering Mechanics, Karlsruhe Institute of Technology, Kaiserstraße 10, Karlsruhe, Baden-Württemberg, Germany

Correspondence
Jimmy Aramendiz, KIT-Campus South, Institute of Engineering Mechanics, Chair for Dynamics/Mechatronics, Bld. 10.23, R. 206.2, Kaiserstraße 10, 76131 Karlsruhe.
Email: jimmy.aramendiz@kit.edu

Funding information
Deutsche Forschungsgemeinschaft, Grant/Award Number: Grant FI 1761/2-1

This paper presents two sequential friction-spring damper configurations and develops numerical and analytical models, which describe the systems' behavior. The dampers rely on the non-smooth characteristics of dry friction to quench unwanted oscillations and only dissipate energy once a preset breakaway force of the friction element is exceeded. Since no additional control is required and the dissipation is only present within a given frequency range, this passive amplitude adaptive dissipation contributes to a higher energy efficiency. The dampers' equations of motion are derived and implemented in a numerical model to gain the first insights into the dampers' behavior. These equations of motion are analyzed via averaging methods in combination with a modal decoupling for nonlinear systems, which lead to the dampers' analytical models. The results from both models are compared and show reasonable agreement within the validity range of asymptotic methods. This work proposes two friction based amplitude adaptive dampers and offers a starting point for future experimental validation.

KEYWORDS
averaging method, dry friction, modal decoupling, non-smooth dampers

1 | INTRODUCTION

If modern machines are to meet the standards set by political requirements and become environmentally friendly, efficient mechanical dampers are required. Every percentage increasing the mechanical efficiency of a machine contributes to the fulfillment of these goals. In general, dampers are introduced in machines in order to quench unwanted and also partly unavoidable oscillations in mechanical systems. Although in many cases dampers are designed to maximize energy dissipation, the recent importance of energetic efficiency requires that only as much energy should be dissipated as necessary.

To quench unwanted oscillations most applications rely on introducing damping in a viscous form, e.g hydraulic shock absorbers in the automotive industry,[1] or by increasing the structures' already present material damping, e.g constrained layer damping.[2] This type of damping is always present and therefore constantly dissipating energy, even when this is not required, thus reducing the energy efficiency of the system. However, these are not the only way to introduce dampers into machines. Impact dampers for example rely on collision masses and have been studied in [3–7] mainly in three variations: with clearance, with a singular impact mass, and with multiple impact masses. Impact dampers were also investigated for turbomaschinery in [8]. Closely related to impact dampers are tuned liquid dampers,[9–11] which take advantage of a water tank and sloshing to

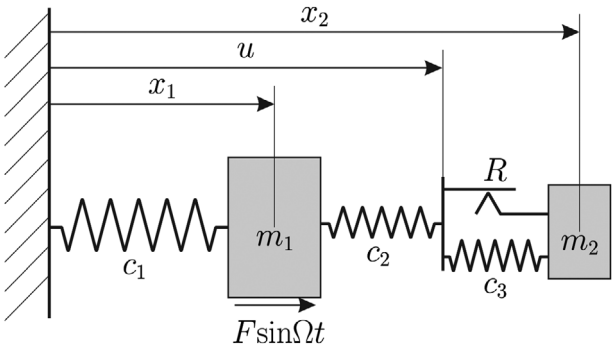

FIGURE 1 Dynamic vibration absorber

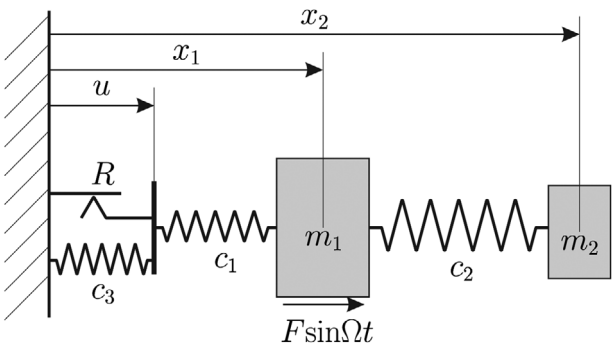

FIGURE 2 Dynamic vibration isolator

reduce the main systems amplitudes. Magneto-electro-rheological dampers[12–15] constitute a damper with actively adjustable parameters, e.g. stiffness and breakaway force. Dampers relying on nonlinear viscous relationships have been studied in [16–18]. Vibration absorbers for turbomachinery were studied in [19,20], whereas dampers based on a nonlinear generalization of Den Hartog's Equal-Peak Method are investigated in [21–24]. Friction dampers are often found in between turbine blades and disks or between the blades themselves.[25–28] Works that model turbine blades as cantilever beams with friction dampers are seen in [28–31]. Furthermore, friction dampers are also implemented in civil engineering structures, e.g beam-to-column joints and in the damping of cable oscillations, as presented in [32–34].

In [35] a friction damper based on a sequential friction-spring element is proposed and studied. The proposed damper is able to reduce the amplitudes of the main mass in two different scenarios: in the case of external force excitation and in the case of self-excitation due to a negative friction gradient. Additionally, it was found that the amplitude reduction effect mainly comes from the switching between the system's two eigenfrequencies, one in the stick-phase and one in the slip-phase.

This work studies the effects of such an sequential friction-spring element in a two mass system in different arrangements. The stick-slip behavior of dry friction is taken into account and used to generate a local energy dissipation in a given frequency regime. The ideas proposed in the work are based on the sequential friction-spring element proposed in [35]. In Section 2 the equations of motion describing both dampers are derived, and an estimate of the domain of the systems' structural change is presented. A numerical model and parameters studies of the system are shown in Section 3. In Section 4 the equations of motion of the proposed dampers are analyzed based on averaging methods and a modal decoupling method presented in [36]. Additionally characteristic values of the system are derived and the analytical and numerical results are compared. Finally, the conclusions of this work are summarized in Section 5.

2 | CONSIDERED SYSTEMS: DAMPER DESCRIPTION AND EQUATIONS OF MOTION

This work presents two friction based dampers: a dynamic vibration absorber (Figure 1) and a dynamic vibration isolator (Figure 2). These dampers differ in the placement of the sequential friction-spring element, which is composed by a sequential arrangement of an second spring and a parallel arrangement of a dry friction and a third spring (c_3). The third spring is only active while the dry friction slides. This sequential element contains the dry friction and thus determines the stick-slip behavior of the dampers. Independent from the friction element the second spring (c_2) is always active. In contrast the third spring has

an influence on the system dynamics only when the dry friction allows a relative movement. The friction force model used in the present paper is described through the simple Coulomb friction. Therefore, the friction coefficient and normal load remain constant in the friction element, and a difference between sticking and sliding friction coefficients is neglected. This result in a non-smooth model of the Fillipov-type,[37,38] where different equations of motion are implemented for the sticking and sliding motions. Once the friction element allows a relative movement the stiffness of the system changes from solely the second spring stiffness to a lower stiffness, which is given by sequential arrangement of the second and third springs. This leads to a change in the eigenfrequencies of the system. Both dampers have a linear and nonlinear ranges, which are respectively determined by the sticking and sliding state of the friction element. The dampers aim to improve the dynamic behavior of a primary system (first spring c_1, first mass particle m_1) combined with a tuned vibration absorber (second spring c_2, second mass particle m_2) attached to it. The behavior improvement is achieved by replacing either the first or second spring with the sequential friction-spring element, allowing the sequential element to react either to the absolute motion of the first mass or the relative motion between the masses respectively. The following subsection presents the equations of motion of both absorbers and derives an estimate for the structural change between the linear sticking system and the nonlinear stick-slip motion.

2.1 | Dynamic vibration absorber

The dynamic vibrations absorber is composed of two masses m_1 and m_2. The first mass is connected to the environment via the first spring c_1, whereas the second mass is attached to the first one via the sequential friction-spring element. The friction-spring element is composed of the second spring c_2, the third spring c_3, and the dry friction R. The position of the masses m_1 and m_2 are respectively described by the coordinates x_1 and x_2, and the coordinate u describes the connecting point in the friction-spring element.

The dynamics of this damper are characterized by two discrete states: a stick-phase and a slip-phase. The system finds itself in the stick-phase, as long as the magnitude of the stiction force H is smaller than the breakaway force R ($|H| \leq R$) and the kinematic condition $\dot{u} = \dot{x}_2$ is fulfilled. Once the kinematic condition is broken, the dry friction element slides, allows a relative motion, and dissipates energy. The equations of motion for both phases are given as follows

$$\text{stick} - \text{phase}: \quad \begin{cases} m_1\ddot{x}_1 + c_1x_1 + c_2(x_1 - u) = F\sin\Omega t \\ m_2\ddot{x}_2 + c_2(u - x_1) = 0 \\ H = c_2(u - x_1) - c_3(x_2 - u) \end{cases}, \tag{1}$$

$$\text{slip} - \text{phase}: \quad \begin{cases} m_1\ddot{x}_1 + c_1x_1 + c_2(x_1 - u) = F\sin\Omega t \\ m_2\ddot{x}_2 + c_3(x_2 - u) + R\text{sign}(\dot{x}_2 - \dot{u}) = 0 \\ (c_2 + c_3)u = c_2x_1 + c_3x_2 + R\text{sign}(\dot{x}_2 - \dot{u}) \end{cases}. \tag{2}$$

The sticking phase is described by two equations of motion and a constraint force equation, whereas the slip-phase is described by two equations of motion and a third equation for u. The variable u does not have its own dynamics and thus $\text{sgn}(\dot{x}_2 - \dot{u}) = \text{sgn}(\dot{x}_2 - \dot{x}_1)$. Introducing this relation in the equation for u yields an algebraic equation and therefore u is considered a slave variable.[39]

As shown in [36], it is intuitive, that the nonlinear frequency-response curve will remain on that of the sticking system until a given breakaway amplitude, followed by a nonlinear range, and finalized again on the frequency-response curve of the sticking system. Since the nonlinearities in this system are only present in the slip-phase, the solution of Equation (1) is obtained with linear methods. Furthermore, an estimate of the breakaway amplitude is derived with the linear solution, for a detailed description see Appendix A. Introducing the solution of the linear system into $|H| \leq R$ in combination with the triangle inequality yields a frequency dependent limit amplitude $A_L(\Omega)$

$$|H| = |c_2(u - x_1) - c_3(x_2 - u)| \leq R, \tag{3}$$

$$\text{with} \quad x_1 = A_1(\Omega), \quad x_2 = \frac{A_1(\Omega)c_2}{c_2 - m_2\Omega^2}, \quad u = x_2 - w_0 \quad \& \quad w_0 = \text{const.}, \tag{4}$$

$$A_1(\Omega) \leq A_L(\Omega) = \left|\frac{m_2\Omega^2 - c_2}{m_2\Omega^2c_2}\right|(R - (c_2 + c_3)|w_0|). \tag{5}$$

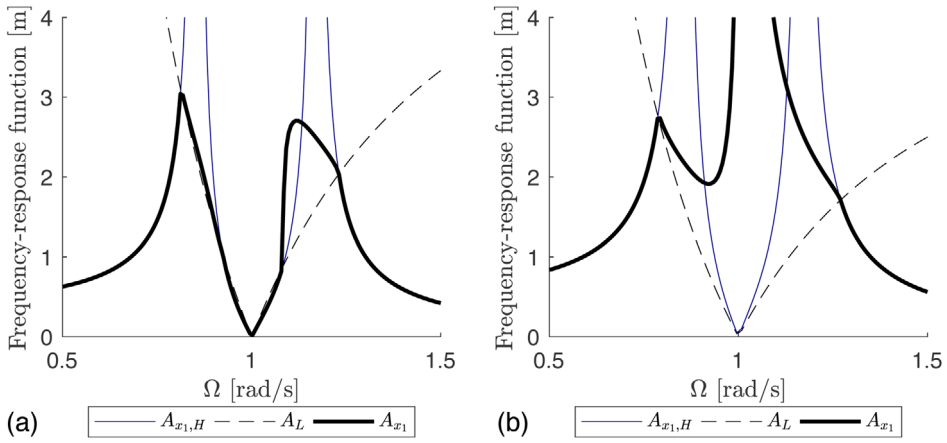

FIGURE 3 Structural change estimation for $w_0 = 0$. (a) Exemplary case with three linear ranges and two nonlinear ranges with standard parameters and $R = 0.60$ N and $F = 0.45$ N. (b) Exemplary case with two linear ranges and one nonlinear range with standard parameters and $R = 0.45$ N and $F = 0.60$ N

Since the triangle inequality is applied, $A_L(\Omega)$ is a conservative estimate. Thus the Amplitudes below $A_L(\Omega)$ correspond to the linear system; the ones above can correspond to the nonlinear system and are yet to be determined. Considering that the limit amplitude is per definition positive, Equation (5) yields a maximum value for the relative displacement w_0 in the sequential friction-spring element. The limit curve for two exemplary cases are plotted in Figure 3. These cases are generated using the numerical models and standard parameters listed in Section 3. Only the breakaway force R and excitation amplitude F were varied. These cases represent two qualitatively different scenarios, which differ through the existence of an antiresonance frequency. An antiresonance frequency is achieved, when the system is completely in the stick-phase at the frequency $\Omega_{\mathrm{AR}} = \sqrt{c_2/m_2}$. Therefore, the frequency Ω_{AR} should belong to the linear range. The linear and nonlinear ranges are determined by the intersections of the limit curve and the frequency-response curve of the sticking system. The limit curve in Figure 3(a) intersects the frequency-response curve of the sticking system $A_{x_1,H}$ four times leading to three linear ranges and two nonlinear ranges, whereas the curve in Figure 3(b) only intersects the linear system at two frequencies. As mentioned above, the main qualitative difference between these two systems lies in the antiresonance frequency in case (a), due to the linear range in the vicinity of Ω_{AR}. This linear range is achieved when four intersections of the limit curve and the frequency response are found. To this end the slopes of the limit curve are chosen higher than that of the linear system at the antiresonant frequency. This is a helpful characteristic, when designing such dampers. The existence condition for an antiresonance frequency yields

$$R \geq F. \tag{6}$$

An last possible scenario includes a system with an antiresonance frequency and unbounded amplitudes, in contrast to Figure 3(a). This occurs a the nonlinear stick-slip motion occurs at an eigenfrequency of the slipping system. In order to avoid unbounded amplitudes, the linear sticking range should include the eigenfrequencies of the slipping system.

2.2 | Dynamic vibration isolator

Analogously to the dynamic vibration absorber in Section 2.1 the dynamic vibration isolator is also composed of two masses. In this arrangement the first mass m_1 is supported by the sequential friction-spring element (c_1, c_3, and R). The second mass is attached to the first via the second spring c_2. As with the first damper, the motion of the dynamic vibration isolator is characterized by the stick-phase and the slip-phase, which are described by

$$\text{stick} - \text{phase}: \quad \begin{cases} m_1\ddot{x}_1 + c_1(x_1 - u) + c_2(x_1 - x_2) = F\sin\Omega t \\ m_2\ddot{x}_2 + c_2(x_2 - x_1) = 0 \\ H = c_1(x_1 - u) - c_3 u \end{cases} \tag{7}$$

$$\text{slip} - \text{phase}: \quad \begin{cases} m_1\ddot{x}_1 + c_1(x_1 - u) + c_2(x_1 - x_2) = F\sin\Omega t \\ m_2\ddot{x}_2 + c_2(x_2 - x_1) = 0 \\ R\,\mathrm{sgn}(\dot{x}_1) + c_3 u = c_1(x_1 - u) \end{cases}. \tag{8}$$

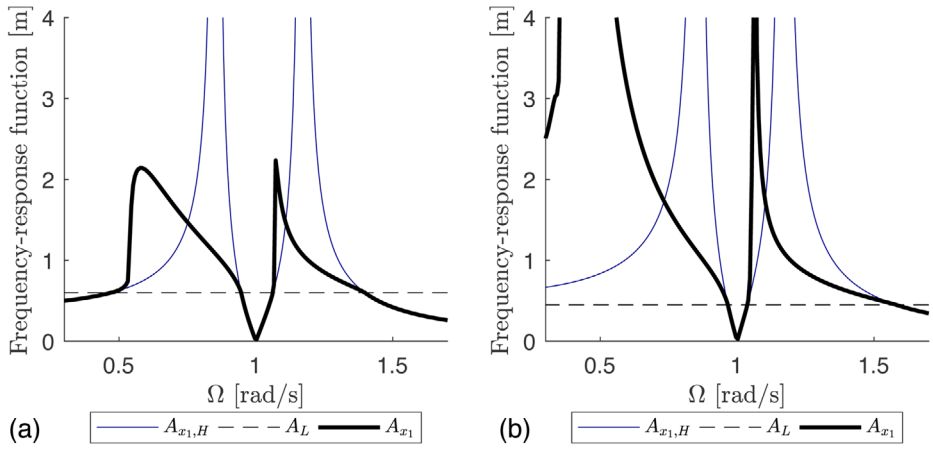

FIGURE 4 Structural change estimation for $u_0 = 0$. (a) Exemplary case with limited frequency-response function with standard parameters and $c_3 = 0.25$ N/m, $R = 0.60$ N and $F = 0.45$ N. (b) Exemplary case without limited frequency-response function with standard parameters and $c_3 = 0.25$ N/m, $R = 0.45$ N and $F = 0.60$ N

Although the equations of motion in Equations (7) and (8) are similar, they differ fundamentally because of the variable u. Since the dry-friction element prevents relative movement in the stick-phase, u is constant throughout this phase, whereas the variable u in the slip-phase is determined by the algebraic equation in Equation (8). In this case the variable u is also a slave variable. Using the same method as in Subsection 2.1, see Appendix A the limit amplitude A_L for this case is derived

$$A_1(\Omega) \leq A_L = \frac{R - (c_1 + c_3)|u_0|}{c_1}, \quad \text{with } |u_0| \leq \frac{R}{c_1 + c_3}. \tag{9}$$

In this case the limit amplitude, which separates the linear and nonlinear systems, does not depend on the excitation frequency. It is a constant value depending on the breakaway force R, the springs c_1 and c_3, and the prestress u_0. It is observed that as long as $A_L > 0$ the frequency-response curve of the dynamic vibration isolator always has three linear ranges that are separated by two nonlinear ranges. The two possible, qualitatively different scenarios are considered in Figure 4. These differ by the bounded and unbounded vibration amplitudes. As in Section 2.1, the linear range of the dynamic vibration isolator should include the eigenfrequencies of the slipping system, in order to avoid large amplitudes in the nonlinear range. Furthermore, for $A_L > 0$ an antiresonance frequency always exists.

3 | NUMERICAL MODEL AND PARAMETER STUDIES

In order to obtain a first insight into the dynamics of the dampers a numerical model is developed. The numerical simulations take into account the stick-slip phases with the help of a Karnopp-friction model.[40] The periodic solution of the dampers is obtained with a shooting method.[41] Afterwards, parameter studies for the breakaway force R and the third spring c_3 are made.

3.1 | Implementation of the numerical model

The numerical model is derived in this subsection for the dynamic vibration absorber and can be analogously obtained for the dynamic vibration isolator. Using the Karnopp-friction model a vicinity 2ν of small relative velocities $v_{\text{rel}} = \dot{x}_2 - \dot{u}$ of the sequential spring element is defined. This simplifies the numerical handling of the relative velocity zero-crossing and yields for the dynamic vibration absorber a friction force defined in a piecewise manner:

$$F_{\text{friction}} = \begin{cases} H = c_2(u - x_1) - c_3(x_2 - u), & |\dot{x}_2 - \dot{u}| \leq \nu \text{ and } |H| \leq R \\ R\text{sgn}(\dot{x}_2 - \dot{u}), & \text{else} \end{cases}. \tag{10}$$

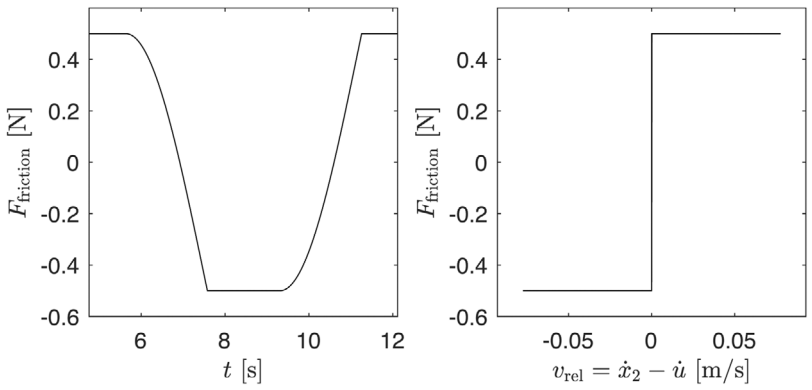

FIGURE 5 Friction Force vs. time (left) and friction force vs. relative velocity $v_{\text{rel}} = \dot{x}_2 - \dot{u}$ for the dynamic vibration absorber. With $m_1 = 1\text{kg}$, $m_2 = 0.1\text{kg}$, $c_1 = 1\text{N/m}$, $c_2 = 0.1\text{N/m}$, $c_3 = 10\text{N/m}$, $R = 0.5$ $F = 0.01\text{N}$, $\Omega = 0.854$ rad/s, $\nu = 1\text{e} - 10$

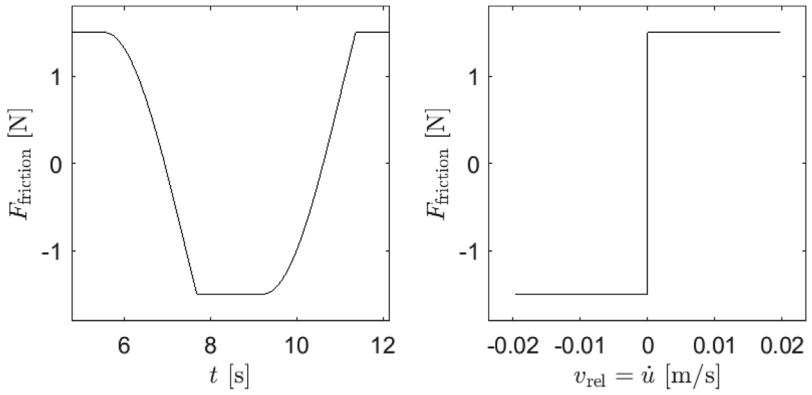

FIGURE 6 Friction Force vs. time (left) and friction force vs. relative velocity $v_{\text{rel}} = \dot{x}_2 - \dot{u}$ for the dynamic vibration isolator. With $m_1 = 1\text{kg}$, $m_2 = 0.1\text{kg}$, $c_1 = 1\text{N/m}$, $c_2 = 0.1\text{N/m}$, $c_3 = 100\text{N/m}$, $R = 1.5$ $F = 0.01\text{N}$, $\Omega = 0.854$ rad/s, $\nu = 1\text{e} - 10$

Introducing this force in the system yields piecewise defined equations of motion

$$\begin{cases} m_1\ddot{x}_1 + c_1x_1 + c_2(x_1 - u) = F\sin\Omega t \\ m_2\ddot{x}_2 + c_2(u - x_1) = 0 \\ u = x_2 - w_0,\ w_0 = \text{const.} \end{cases}, \quad |\dot{x}_2 - \dot{u}| \le \nu \text{ and } |c_2(u - x_1) - c_3(x_2 - u)| \le R$$
$$\begin{cases} m_1\ddot{x}_1 + c_1x_1 + c_2(x_1 - u) = F\sin\Omega t \\ m_2\ddot{x}_2 + c_3(x_2 - u) + R\text{sgn}(\dot{x}_2 - \dot{u}) = 0 \\ u = (c_2x_1 + c_3x_2 + R\text{sign}(\dot{x}_2 - \dot{u}))/(c_2 + c_3) \end{cases}, \quad \text{else} \qquad (11)$$

Applying the identical procedure to the equations of motion of the dynamic vibration isolator yields

$$F_{\text{friction}} = \begin{cases} H = c_1(x_1 - u) - c_3u, & |\dot{u}| \le \nu \text{ and } |H| \le R \\ R\text{sgn}(\dot{u}), & \text{else} \end{cases} \qquad (12)$$

for the piecewise friction force and the piecewise equations of motion are given as

$$\begin{cases} m_1\ddot{x}_1 + c_1(x_1 - u) + c_2(x_1 - x_2) = F\sin\Omega t \\ m_2\ddot{x}_2 + c_2(x_2 - x_1) = 0 \\ u = \text{const.} \end{cases}, \quad |\dot{u}| \le \nu \text{ and } |H| \le R$$
$$\begin{cases} m_1\ddot{x}_1 + c_1(x_1 - u) + c_2(x_1 - x_2) = F\sin\Omega t \\ m_2\ddot{x}_2 + c_2(x_2 - x_1) = 0 \\ u = (c_1 - R\text{sgn}(\dot{x}_1))/(c_1 + c_3) \end{cases}, \quad \text{else} \qquad (13)$$

Figures 5 and 6 show the friction force plotted against the time and the relative velocity of the friction element. The friction forces are calculated using Equations (10) and (12) for the dynamic vibration absorber and the dynamic vibration isolator

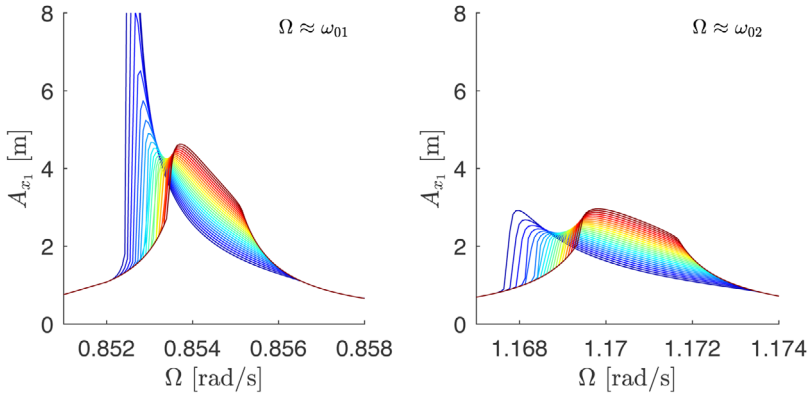

FIGURE 7 Parameter study: dynamic vibration absorber - breakaway force $R \in [0.3\text{N(blue)}, 0.8\text{N(red)}]$ in steps of 0.02 N. With $m_1 = 1\text{kg},\ m_2 = 0.1\text{kg},\ c_1 = 1\text{N/m},\ c_2 = 0.1\text{N/m},\ c_3 = 10\text{N/m},\ F = 0.01\text{N}$

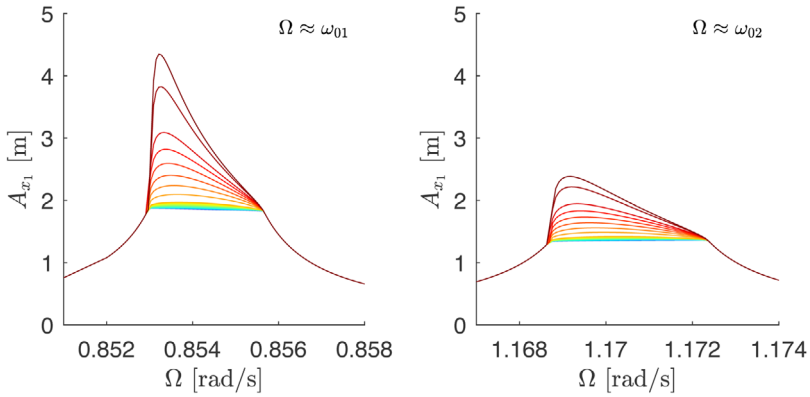

FIGURE 8 Parameter study: dynamic vibration absorber - stiffness $c_3 \in [0.01\text{N/m(blue)}, 10\text{N/m(red)}]$ in steps of 0.01 N/m until 1 N/m afterwards in steps of 1N/m. With $m_1 = 1\text{kg},\ m_2 = 0.1\text{kg},\ c_1 = 1\text{N/m},\ c_2 = 0.1\text{N/m},\ R = 0.5\text{N},\ F = 0.01\text{N}$

respectively. The excitation frequency of $\Omega = 0.854$ rad/s was chosen with the nonlinear stick-slip range of the first eigenfrequency. Despite the high inertia forces present in the resonance regime, noticeable stick- and slip-phases are observed. Both oscillations are characterized by two stick-phases and two slip phases, with continuous transitions, as is common for a Coulomb friction model.

In order to obtain the frequency-response function of the system, the periodic solution for each excitation frequency is needed. To this end a shooting method is implemented in which the necessary derivatives are calculated numerically.[41] Both dampers introduce the third spring c_3 and the breakaway force R as additional parameters in the system. Since the second mass particle m_2 and second spring c_2 are tuned with respect to the main mass particle, only the newly introduced parameters can be freely chosen. Thus, only the two above mentioned parameters are studied. Since the improvement of the main system's dynamics has a higher priority the parameter studies are focused mainly on the first coordinate x_1. The results for the second coordinate x_2 are presented in Appendix B.

3.2 | Parameter study: Dynamic vibration absorber

The left plot in Figure 7 corresponds to the frequency-response function of the coordinate x_1 in the vicinity of the first eigenfrequency, and accordingly the second eigenfrequency is observed in the right plot. For selected values of R the damper is able to limit the amplitudes in the frequency-response function, although the dissipated energy is only proportional to the amplitude of the relative movement. The amplitudes for the second eigenfrequency are noticeably lower than that for the first eigenfrequency. This is due to the corresponding eigenmode for each resonance regime. In the vicinity of the second eigenmode the variables x_1 and x_2 are out of phase leading to higher relative displacements between the two coordinates. With higher relative displacements the sequential friction-spring element is able to dissipate more energy. An additional finding of this parameter study is the existence of an optimal value for the breakaway force R. For the considered friction model this would result in finding the optimal friction coefficient for a given normal load or vice versa, similar investigation are found in [42]. The parameter study in Figure 8 shows the same behavior between the first and second frequencies, which is expected since the sequential friction-spring element still reacts to the relative motion. In contrast to the first parameter study no optimal value for the stiffness c_3 is found. The study shows smaller amplitudes in the frequency-response curve with smaller stiffness values. Correspondingly, the

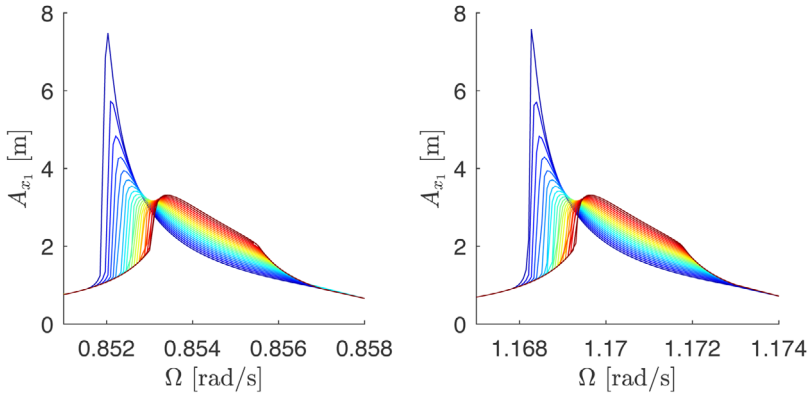

FIGURE 9 Parameter study: dynamic vibration isolator - breakaway force $R \in [0.9\text{N(blue)}, 2.0\text{N(red)}]$ in steps of 0.05 N. With $m_1 = 1\text{kg}$, $m_2 = 0.1\text{kg}$, $c_1 = 1\text{N/m}$, $c_2 = 0.1\text{N/m}$, $c_3 = 100\text{N/m}$, $F = 0.01\text{N}$

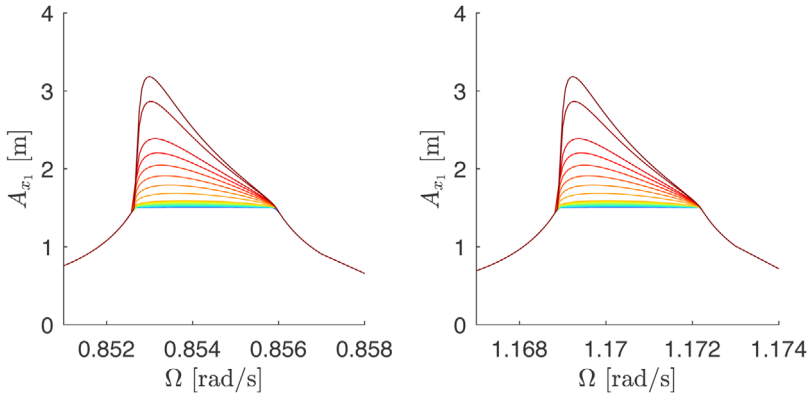

FIGURE 10 Parameter study: dynamic vibration isolator - stiffness $c_3 \in [0.1\text{N/m(blue)}, 100\text{N/m(red)}]$ in steps of 0.1 N/m until 1, afterwards steps of 1 N/m until 10 N/m, and finally steps of 10 N/m until 100 N/m. With $m_1 = 1\text{kg}$, $m_2 = 0.1\text{kg}$, $c_1 = 1\text{N/m}$, $c_2 = 0.1\text{N/m}$, $R = 1.5\text{N}$, $F = 0.01\text{N}$

stiffness of the third spring should be chosen as small as possible. However c_3 should not be equal to zero, since this leads to no change in the eigenfrequency of the system between the sticking and sliding configurations.

3.3 | Parameter study: Dynamic vibration isolator

Analogous to the dynamic vibration absorber both the breakaway force R and the stiffness c_3 are studied. In contrast to the parameter study for the vibration absorber Figure 9 shows an equal damping of both eigenfrequencies. This is expected, since the sequential friction-spring element in this case replaces the first spring and reacts to the absolute movement of the main mass. Therefore it is automatically activate equally at both eigenfrequencies, once the constant limit amplitude is overcome. This parameter study also reveals the existence of an optimal breakaway force. The study of the third spring c_3 shows the same behavior as with the dynamic vibration absorber. Thus, for both systems the highest amplitude reduction is obtained with the highest change between the eigenfrequencies of the linear sticking system and the nonlinear stick-slip system. These dampers just efficiently utilize the basic concept of any vibration absorber.[43]

4 | ANALYTICAL MODEL: COMPLETE MODAL DECOUPLING AND FIRST ORDER AVERAGING

The numerical simulations offer first insights into the influence of the additional parameters. However, they do not offer a deeper insight and require new simulations for each parameter set. This work offers a deeper understanding of these dampers by providing an analytical solution that shows the relationship between the system parameters and the frequency-response function. To this end the systems' equations of motion are transformed and a nonlinear modal decoupling is applied. Afterwards the nonlinear frequency-response function is derived for both dampers via averaging methods.

4.1 | Equations transformations and complete modal decoupling

For the sake of brevity the detailed transformations presented in this section are limited to the dynamic vibration absorber. However, these can be analogously applied to the dynamic vibration isolator. First, a variable transformation is introduced in the equations of motion of the sticking system. Additionally, the equations are nondimensionalized. The following transformations and nondimensional parameters are introduced:

$$\begin{gathered} z_1 = \frac{m_1 x_1 + m_2 x_2}{m_1 + m_2},\ z_2 = x_2 - x_1,\ w = x_2 - u,\ \mu = \frac{m_2}{m_1 + m_2},\ k = \sqrt{\frac{c_1}{m_1}},\ \lambda = \sqrt{\frac{c_2}{m_2}},\ p = \frac{\lambda^2}{k^2}, \\ \tau = kt,\ (\cdot)' = \frac{\mathrm{d}}{\mathrm{d}\tau}(\cdot),\ \eta = \frac{\Omega}{k},\ \varepsilon\kappa = \frac{c_2}{c_2 + c_3},\ \varepsilon\rho = \frac{R}{c_2 + c_3},\ \varepsilon f = \frac{F}{m_1 k^2}, \varepsilon \ll 1. \end{gathered} \tag{14}$$

The coordinate z_1 describes the position of the center of mass of the dual mass system, whereas the second coordinate z_2 describes the relative motion between the masses. The coordinate w describes the relative motion between the ends of the dry friction element. Furthermore it includes the stick-slip behavior in the equations of motion of the system, and is defined in Section 4.2. Additionally, the small parameter ε is introduced. Making use of the parameters in Equation (14), Equation (2) is rewritten in the following form:

$$\begin{gathered} z_1'' + (1-\mu)z_1 - \mu(1-\mu)z_2 = \varepsilon f(1-\mu)\sin\eta\tau = \varepsilon f_{NL,1}(z_1, z_2) \\ z_2'' - z_1 + \left(\mu + \frac{p}{1-\mu}\right) z_2 = \frac{p}{1-\mu} w(z_2) - \varepsilon f \sin\eta\tau = \varepsilon f_{NL,2}(z_1, z_2). \\ w(z_2) = \varepsilon(\kappa z_2 - \rho \mathrm{sgn}(z_2')) \end{gathered} \tag{15}$$

Rewriting this last equation in a compact form with the mass matrix $\boldsymbol{M}$, the stiffness matrix $\boldsymbol{C}$, and the nonlinear vector $\boldsymbol{f}_{NL}(\boldsymbol{z})$ results in

$$\begin{gathered} \boldsymbol{M}\ddot{\boldsymbol{z}} + \boldsymbol{C}\boldsymbol{z} = \varepsilon \boldsymbol{f}_{NL}(\boldsymbol{z}) \\ w(z_2) = \varepsilon(\kappa z_2 - \rho \mathrm{sgn}(z_2')) \end{gathered}. \tag{16}$$

For the sake of generality the nonlinear right hand sides of Equation (15) and (16) are assumed to be functions of system's degrees of freedom. Although the right hand side of Equation (15) is small, the equations cannot be averaged because of the coupling on the left hand side. In order to decouple the system's equations a nonlinear modal decoupling[36,44] is applied. The modal matrix $\boldsymbol{R}$ is calculated based on the linear unperturbed system ($\varepsilon = 0$) and yields the following equations in the modal coordinates q_1 and q_2

$$\begin{gathered} \boldsymbol{R}^T \boldsymbol{M} \boldsymbol{R}\ddot{\boldsymbol{q}} + \boldsymbol{R}^T \boldsymbol{C} \boldsymbol{R}\boldsymbol{q} = \boldsymbol{R}^T \boldsymbol{f}(\boldsymbol{q}), \quad \boldsymbol{R} = \begin{pmatrix} r_{11} & r_{12} \\ r_{21} & r_{22} \end{pmatrix} \\ q_1'' + \eta_1^2 q_1 = \varepsilon(r_{11} f_{NL,1}(q_1, q_2)) + r_{21} f_{NL,2}(q_1, q_2)) \\ q_2'' + \eta_2^2 q_2 = \varepsilon(r_{12} f_{NL,1}(q_1, q_2)) + r_{22} f_{NL,2}(q_1, q_2)) \end{gathered} \tag{17}$$

Equation (17) has a decoupled left hand side, however the right hand side is still coupled due to the nonlinear terms. Each modal coordinate has to be investigated in the vicinity of its corresponding eigenfrequency. Considering the vicinity of the first eigenfrequency, it is clear, at least in linear systems, that the first modal coordinate has much higher amplitudes in the frequency-response curve as the second modal coordinate. The larger the distance is between the eigenfrequencies, the smaller the second modal coordinate is in the resonance regime of the first modal coordinate and vice versa. Since the system is weakly nonlinear, it can be assumed, that it will behave in a similar way. Thus, in the vicinity of the first eigenfrequency the second modal coordinate is neglected for the first order averaging method, since it will have small values ($\mathcal{O}(\varepsilon)$), provided the difference between the eigenfrequencies is sufficiently large. Based on the linear system the procedure is valid as long as $\eta_2 - \eta_1 = \mathcal{O}(1)$,

see Appendix C. This method can be expanded to n-degrees of freedom. Analogously in the vicinity of a certain eigenfrequency only the corresponding modal coordinate is considered and all others are neglected. For Equation (17) this results in

$$\begin{aligned} q_1'' + \eta_1^2 q_1 &= \varepsilon(r_{11} f_{NL,1}(q_1, 0)) + r_{21} f_{NL,2}(q_1, 0)) \\ q_2'' + \eta_2^2 q_2 &= \varepsilon(r_{12} f_{NL,1}(0, q_2)) + r_{22} f_{NL,2}(0, q_2)) \end{aligned} \tag{18}$$

Applying this procedure to the equations of motion of the dynamic vibration absorber leads to

$$\begin{aligned} q_1'' + \eta_1^2 q_1 &= \varepsilon f(\mu - 1)(\mu r_{21} - r_{11}) \sin \eta\tau + \mu p r_{21} w(q_1) \\ q_2'' + \eta_2^2 q_2 &= \varepsilon f(\mu - 1)(\mu r_{22} - r_{12}) \sin \eta\tau + \mu p r_{22} w(q_2) \end{aligned}. \tag{19}$$

Analogously this modal decoupling is used for the equations of the dynamic vibration isolator. The essential equations are summarized below:

$$\begin{aligned} &\mu = \frac{m_2}{m_1 + m_2},\ k = \sqrt{\frac{c_1}{m_1}},\ \lambda = \sqrt{\frac{c_2}{m_2}},\ p = \frac{\lambda^2}{k^2}, \tau = kt,\ (\cdot)' = \frac{\mathrm{d}}{\mathrm{d}\tau}(\cdot), \\ &\eta = \frac{\Omega}{k},\ \varepsilon\kappa = \frac{c_1}{c_1 + c_3},\ \varepsilon\rho = \frac{R}{c_1 + c_3},\ \varepsilon f = \frac{F}{m_1 k^2}, \varepsilon \ll 1. \end{aligned} \tag{20}$$

$$u = \varepsilon(\kappa x_1 - \rho \mathrm{sgn}(\dot{x}_1)) = w \tag{21}$$

$$\begin{aligned} x_1'' + \left(1 + \frac{p\mu}{1 - \mu}\right) x_1 - \frac{p\mu}{1 - \mu} x_2 &= \varepsilon f \sin \eta\tau + w(x_1) \\ x_2'' - p x_1 + p x_2 &= 0 \end{aligned} \tag{22}$$

Decoupling the equations yields

$$\begin{aligned} q_1'' + \eta_1^2 q_1 &= \varepsilon r_{11} f \sin \eta\tau + r_{11} w(q_1) \\ q_2'' + \eta_2^2 q_2 &= \varepsilon r_{21} f \sin \eta\tau + r_{21} w(q_2) \end{aligned} \tag{23}$$

4.2 | First order averaging: Dynamic vibration absorber

The first order averaging method leads to the analytic expressions that describe the frequency-response function. To this end, the equations are first brought in standard form with the help of a Van-der-Pol-transformation. Second, an expression for the variable w is obtained depending on the corresponding phase angle. Third, the motion of the system is separated into the slow changing dynamics of the system and the fast pace oscillations. Subsequently the equations are averaged and the resulting expressions for the frequency-response curve are analyzed. The Van-der-Pol transformation is introduced for each modal coordinate for both systems in the form

$$\begin{aligned} q_1 &= A_1 \sin \varphi_1, \quad \dot{\varphi}_1 = A_1 \eta_1 \cos \varphi_1 \\ q_2 &= A_2 \sin \varphi_2, \quad \dot{\varphi}_2 = A_2 \eta_2 \cos \varphi_2 \end{aligned}. \tag{24}$$

Additionally, each line of Equation (19) is investigated in the vicinity of the corresponding eigenfrequency, which implies that the difference between the considered eigenfrequency and the excitation frequency is small, i.e. $\eta_1 - \eta = \varepsilon\delta_1$ and $\eta_2 - \eta = \varepsilon\delta_2$. Furthermore, the slowly changing phase differences $\psi_1 = \varphi_1 - \eta\tau$ and $\psi_2 = \varphi_2 - \eta\tau$ are introduced. This yields the system in

the standard form for averaging

$$
\begin{aligned}
A_1' &= \frac{\mu p r_{21}}{\eta_1} w(q_1)\cos\varphi_1 - \varepsilon\frac{(1-\mu)(r_{21}\mu - r_{11})\sin(\psi_1-\varphi_1)}{\eta_1} f\cos\varphi_1 \\
\psi_1' &= \varepsilon\delta_1 - \frac{\mu p r_{21}}{A_1\eta_1} w(q_1)\sin\varphi_1 + \varepsilon\frac{(1-\mu)(r_{21}\mu - r_{11})\sin(\psi_1-\varphi_1)}{A_1\eta_1} f\sin\varphi_1, \\
\varphi_1' &= \eta_1 - \frac{\mu p r_{21}}{A_1\eta_1} w(q_1)\sin\varphi_1 + \varepsilon\frac{(1-\mu)(r_{21}\mu - r_{11})\sin(\psi_1-\varphi_1)}{A_1\eta_1} f\sin\varphi_1
\end{aligned} \tag{25}
$$

$$
\begin{aligned}
A_2' &= \frac{\mu p r_{22}}{\eta_2} w(q_2)\cos\varphi_2 - \varepsilon\frac{(1-\mu)(r_{22}\mu - r_{12})\sin(\psi_2-\varphi_2)}{\eta_2} f\cos\varphi_2 \\
\psi_2' &= \varepsilon\delta_2 - \frac{\mu p r_{22}}{A_2\eta_2} w(q_2)\sin\varphi_2 + \varepsilon\frac{(1-\mu)(r_{22}\mu - r_{12})\sin(\psi_2-\varphi_2)}{A_2\eta_2} f\sin\varphi_2. \\
\varphi_2' &= \eta_2 - \varepsilon\frac{\mu p r_{22}}{A_2\eta_2} w(q_2)\sin\varphi_2 + \varepsilon\frac{(1-\mu)(r_{22}\mu - r_{12})\sin(\psi_2-\varphi_2)}{A_2\eta_2} f\sin\varphi_2
\end{aligned} \tag{26}
$$

In order to evaluate Equation (25) and (26), an explicit form for $w(q_i)$ is required. Using Equation (15) a piecewise function is defined for $w(q_i)$. This function contains two constant sections that describe the stick phases and two q_i (i.e A_i, φ_i) dependent sections that describe the slip-phases. Based on [35] and depending on the modal coordinate the nondimensionalized relative motion of the dry friction is defined as

$$
w(q_i) = \varepsilon\begin{cases} -\kappa r_{2i}A_i + \rho, & -\pi/2 \le \varphi < \varphi_{r,i} \\ \kappa r_{2i}A_i\sin\varphi_i - \rho, & \varphi_{r,i} \le \varphi < \pi/2 \\ \kappa r_{2i}A_i - \rho, & \pi/2 \le \varphi < \pi + \varphi_{r,i} \\ \kappa r_{2i}A_i\sin\varphi_i + \rho, & \pi + \varphi_{r,i} \le \varphi < 3/2\,\pi \end{cases} \quad \text{with} \quad \varphi_{r,i} = \begin{cases} \varphi_{r,1} = \arcsin\left(1 - \dfrac{2\rho}{\kappa r_{21}A_1}\right) \\ \varphi_{r,2} = \arcsin\left(1 - \dfrac{2\rho}{\kappa r_{22}A_2}\right) \end{cases} \tag{27}
$$

The angles $\varphi_{r,i}$ determine the transitions between the sticking and sliding system and are calculated with the continuity condition for the function $w(q_i)$. Having determined an expression for the function $w(q_i)$, Equation (25) and (26) are averaged over the corresponding phase angle φ_i. In order to distinguish between the general motion and the slowly changing motion, the slow changing variables are denoted with a bar e.g $\bar{A}_i$. Averaging these equations yields

$$
\begin{aligned}
\bar{A}_1' &= \left\langle A_1' \right\rangle_{\varphi_1} = \frac{\varepsilon}{\eta_1}\left(\zeta_{w_1,\cos} - \frac{(\mu-1)(\mu r_{21} - r_{11})\sin\psi_1}{2\eta_1} f\right) \\
\bar{\psi}_1' &= \left\langle \psi_1' \right\rangle_{\varphi_1} = \frac{\varepsilon}{\eta_1}\left(\delta_1 + \zeta_{w_1,\sin} - \frac{(\mu-1)(r_{21}\mu - r_{11})\cos\psi_1}{2\bar{A}_1\eta_1} f\right)
\end{aligned} \tag{28}
$$

$$
\begin{aligned}
\bar{A}_2' &= \left\langle A_2' \right\rangle_{\varphi_2} = \frac{\varepsilon}{\eta_2}\left(\zeta_{w_2,\cos} - \frac{(\mu-1)(\mu r_{22} - r_{12})\sin\psi_2}{2\eta_2} f\right) \\
\bar{\psi}_2' &= \left\langle \psi_2' \right\rangle_{\varphi_2} = \frac{\varepsilon}{\eta_2}\left(\delta_2 + \zeta_{w_2,\sin} - \frac{(\mu-1)(r_{22}\mu - r_{12})\cos\psi_2}{2\bar{A}_2\eta_2} f\right)
\end{aligned} \tag{29}
$$

with

$$
\begin{aligned}
\zeta_{w_1,\cos} &= -2\,\frac{\mu\, p\rho\left(\kappa r_{21}\,\bar{A}_1 - \rho\right)}{\kappa\bar{A}_1\eta_1\,\pi} \\
\zeta_{w_1,\sin} &= -\frac{\mu\, p}{4\kappa\bar{A}_1^2\pi\eta_1}\left(\kappa^2 r_{21}^2\bar{A}_1^2\left(\pi + 2\arcsin\left(\frac{\kappa r_{21}\bar{A}_1 - 2\rho}{\kappa r_{21}\bar{A}_1}\right)\right) + \left(4\kappa r_{21}\bar{A}_1 - 8\rho\right)\sqrt{\rho(\kappa r_{21}\,\bar{A}_1 - \rho)}\right)
\end{aligned} \tag{30}
$$

$$\zeta_{w_2,\cos} = -2\,\frac{\mu\, p\rho\left(\kappa r_{22}\,\bar{A}_2 - \rho\right)}{\kappa \bar{A}_2 \eta_2\,\pi}$$

$$\zeta_{w_2,\sin} = -\frac{\mu\, p}{4\kappa \bar{A}_2^2 \pi \eta_2}\left(\kappa^2 r_{22}^2 \bar{A}_2^2\left(\pi + 2\arcsin\left(\frac{\kappa r_{22}\bar{A}_2 - 2\rho}{\kappa r_{22}\bar{A}_2}\right)\right) + \left(4\kappa r_{22}\bar{A}_2 - 8\rho\right)\sqrt{\rho(\kappa r_{22}\,\bar{A}_2 - \rho)}\right). \tag{31}$$

Calculating the stationary solution ($\bar{A}_1' = 0, \bar{\psi}_1' = 0$) yields an implicit function for the frequency-response curve in the vicinity of the first eigenfrequency

$$\eta = \eta_1 + \varepsilon\zeta_{w_1,\sin} \pm \frac{\varepsilon}{2\bar{A}_1\eta_1}\sqrt{f^2(\mu-1)^2(\mu r_{21} - r_{11})^2 - 4\zeta_{w_1,\cos}^2\eta_1^2}. \tag{32}$$

Analyzing the existence conditions of Equation (32) yields characteristic values of the system's nonlinear dynamics

$$\Im\left\{\sqrt{\rho(\kappa r_{21}\bar{A}_1 - \rho)}\right\} = 0 \;\Rightarrow\; \bar{A}_{1,\min 1} = \frac{\rho}{\kappa r_{21}}, \tag{33}$$

$$\Im\left\{\sqrt{f^2(\mu-1)^2(\mu r_{21} - r_{11})^2 - 4\zeta_{w_1,\cos}^2\eta_1^2}\right\} = 0 \;\Rightarrow\; \begin{aligned} \bar{A}_{1,\min 2} &= \frac{4\mu p\rho^2}{\kappa\left(4\mu p r_{21}\rho + f(\mu-1)(\mu r_{21} - r_{11})\pi\right)} \\ \bar{A}_{1,\max} &= \frac{4\mu p\rho^2}{\kappa\left(4\mu p r_{21}\rho - f(\mu-1)(\mu r_{21} - r_{11})\pi\right)} \end{aligned}, \tag{34}$$

$$\bar{A}_{1,\max} > 0 \;\Rightarrow\; \rho_{1,\min} = \frac{f(\mu-1)(\mu r_{21} - r_{11})\pi}{4\mu p r_{21}}, \tag{35}$$

$$\bar{A}_{1,\min} = \max(\bar{A}_{1,\min 1}, \bar{A}_{1,\min 2}). \tag{36}$$

Additionally, by deriving the maximum amplitude with respect to the nondimensional friction leads to an expression for the optimal friction value

$$\rho_{1,\mathrm{opt}} = \frac{f(\mu-1)(\mu r_{21} - r_{11})\pi}{2p\mu r_{21}}. \tag{37}$$

Calculating the stationary solution ($\bar{A}_2' = 0, \bar{\psi}_2' = 0$) yields

$$\eta = \eta_2 + \varepsilon\zeta_{w_2,\sin} \pm \frac{\varepsilon}{2\bar{A}_2\eta_2}\sqrt{f^2(\mu-1)^2(\mu r_{22} - r_{12})^2 - 4\zeta_{w_2,\cos}^2\eta_2^2}. \tag{38}$$

Analogously an analysis of Equation (38) results in

$$\bar{A}_{2,\min 1} = \frac{\rho}{\kappa r_{22}}, \tag{39}$$

$$\bar{A}_{2,\min 2} = \frac{4\mu p\rho^2}{\kappa\left(4\mu p r_{22}\rho + f(\mu-1)(\mu r_{22} - r_{12})\pi\right)}, \tag{40}$$

$$\bar{A}_{2,\max} = \frac{4\mu p\rho^2}{\kappa\left(4\mu p r_{22}\rho - f(\mu-1)(\mu r_{22} - r_{12})\pi\right)}, \tag{41}$$

$$\bar{A}_{2,\min} = \max(\bar{A}_{2,\min 1}, \bar{A}_{2,\min 2}), \tag{42}$$

$$\rho_{2,\min} = \frac{f(\mu-1)(\mu r_{22} - r_{12})\pi}{4\mu p r_{22}}, \tag{43}$$

$$\rho_{2,\mathrm{opt}} = \frac{f(\mu-1)(\mu r_{22} - r_{12})\pi}{2p\mu r_{22}}. \tag{44}$$

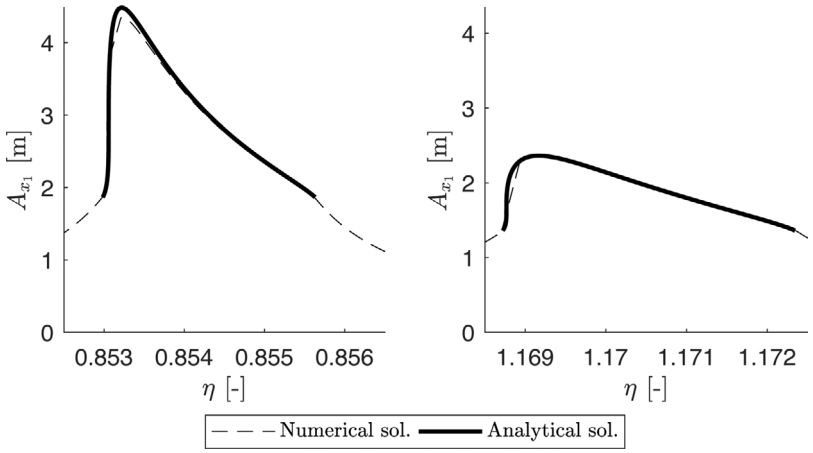

FIGURE 11 Dynamic vibration absorber comparison. With $m_1 = 1\text{kg},\ m_2 = 0.1\text{kg},\ c_1 = 1\text{N/m},\ c_2 = 0.1\text{N/m},\ c_3 = 10\text{N/m},\ R = 0.5\text{N},\ F = 0.01\text{N} \rightarrow \mu = 0.1, \varepsilon = 0.01,\ \kappa = 0.99,\ \rho = 4.95,\ f = 1$

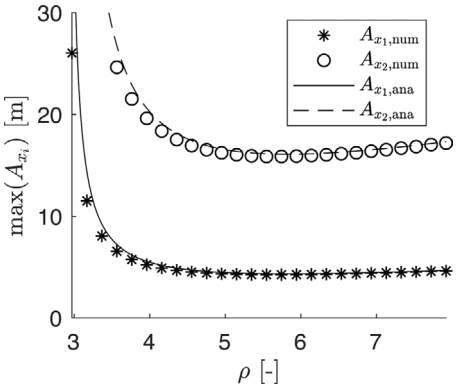

FIGURE 12 Maximum amplitude comparison: Dynamic vibration absorber. With $m_1 = 1\text{kg},\ m_2 = 0.1\text{kg},\ c_1 = 1\text{N/m},\ c_2 = 0.1\text{N/m},\ c_3 = 10\text{N/m},\ F = 0.01\text{N} \rightarrow \mu = 0.1, \varepsilon = 0.01,\ \kappa = 0.99,\ f = 1$

Two optimal nondimensional friction that each minimize the corresponding resonance peak are obtained. However, since as seen in Section 3.2 the first peak of the dynamic vibration absorber is much higher than the second one, the first nondimensional friction value is the decisive optimal value.

Having derived the nonlinear solution for the modal coordinates, all that is left is the reconstruction of the solution in the original coordinates x_1 and x_2. To this end the following transformations are applied

$$\eta \approx \eta_1 \ \Rightarrow \begin{cases} A_{x_1} \approx \sqrt{\bar{A}_1^2(\mu r_{21} - r_{11})^2} \\ A_{x_2} \approx \sqrt{\bar{A}_1^2(\mu r_{21} - r_{11} - r_{21})^2} \end{cases}, \tag{45}$$

$$\eta \approx \eta_2 \ \Rightarrow \begin{cases} A_{x_1} \approx \sqrt{\bar{A}_2^2(\mu r_{22} - r_{12})^2} \\ A_{x_2} \approx \sqrt{\bar{A}_2^2(\mu r_{22} - r_{12} - r_{22})^2} \end{cases}. \tag{46}$$

The analytical model is validated by a comparison between its results and the results of the numerical model. This examination is limited to the vicinities of the eigenfrequencies, since otherwise the nondimensional frequency difference δ_i lies out of the valid range for the averaging method. The comparison results are presented in Figure 11. The friction force and excitation force ratio in these investigations were chosen in order to efficiently reduce vibration amplitudes at the resonance, cf. Figure 12. An acceptable difference within the range of validity for asymptotic methods is noticed between numerical and analytical solutions. Furthermore, a comparison of the maximal amplitude values between the numerical and analytical results is presented in Figure 12.

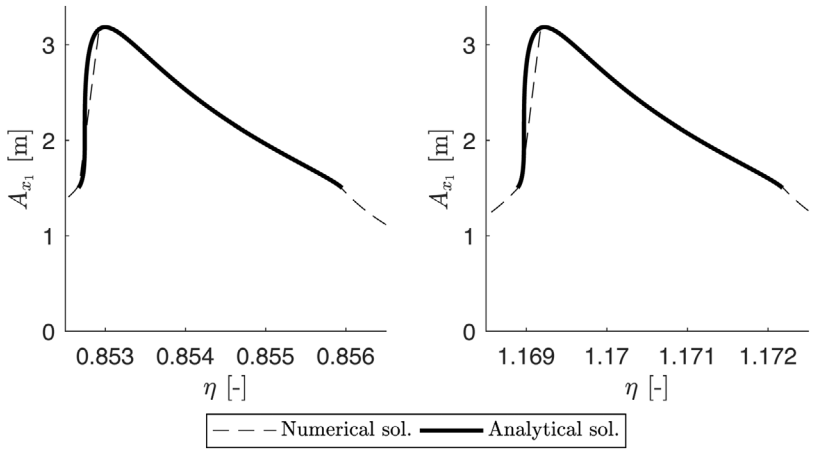

FIGURE 13 Dynamic vibration isolator comparison. With $m_1 = 1\text{kg}$, $m_2 = 0.1\text{kg}$, $c_1 = 1\text{N/m}$, $c_2 = 0.1\text{N/m}$, $c_3 = 100\text{N/m}$, $R = 1.5\text{N}$, $F = 0.01\text{N} \rightarrow \mu = 0.1, \varepsilon = 0.01$, $\kappa = 0.99$, $\rho = 1.49$, $f = 1$

4.3 | First order averaging: Dynamic vibration isolator

The method applied to the equations of motion of the dynamic vibration absorber is similarly applied to the equations of motion of the dynamic vibration isolator. A detailed summary of the equations of this damper is presented in Appendix D. In this section the authors limit themselves to the presentation of both implicit frequency-response curves for each eigenfrequency, the reconstruction functions, and the optimal non dimensional friction value. The implicit frequency-response curve and the amplitudes of the original coordinates are described by

$$\eta = \eta_1 + \varepsilon\zeta_{w_1,\sin} \pm \frac{\varepsilon}{2\bar{A}_1\eta_1}\sqrt{r_{11}^2 f^2 - 4\zeta_{w_1,\cos}^2\eta_1^2}, \tag{47}$$

$$\eta = \eta_2 + \varepsilon\zeta_{w_2,\sin} \pm \frac{\varepsilon}{2\bar{A}_2\eta_2}\sqrt{r_{12}^2 f^2 - 4\zeta_{w_2,\cos}^2\eta_2^2}, \tag{48}$$

$$\eta \approx \eta_1 \Rightarrow \begin{cases} A_{x_1} \approx \bar{A}_1|r_{11}| \\ A_{x_2} \approx \bar{A}_1|r_{21}| \end{cases}, \tag{49}$$

$$\eta \approx \eta_2 \Rightarrow \begin{cases} A_{x_1} \approx \bar{A}_2|r_{12}| \\ A_{x_2} \approx \bar{A}_2|r_{22}| \end{cases}. \tag{50}$$

Deriving and optimal friction value for both modal coordinates results in

$$\rho_{1,\text{opt}} = \rho_{2,\text{opt}} = \frac{\pi f}{2}. \tag{51}$$

Independent analysis of both modal coordinates arrive at the same optimal friction value and is identical to the value found in [35]. This has to be expected, since the sequential friction-spring element reacts, in this case, to the displacement of the absolute coordinate x_1. As well as with the first damper, the analytical solution for the dynamic vibration absorber shows acceptable discrepancy compared to the numerical results, see Figure 13. As with the investigations into the dynamic vibration absorber the magnitudes of the breakaway force and the excitation forces where chosen in order to effectively reduce vibration amplitudes.

5 | CONCLUSIONS

This work proposed two novel implementations of the amplitude-adaptive sequential friction-spring dampers and described their behavior with numerical and analytical models. The working principle of these dampers relies on alternating frequencies between the sticking and slipping systems, whereas conventional systems rely mainly on the dissipation achieved by the friction contact. Springs in series with friction elements can also lead the activation and deactivation of a third spring. However, these arrangements have a practical disadvantage in the case of an asymmetrical excitation, e.g. $F(t) = F_0 + F\sin(\Omega t)$. In such cases

the relative displacement of the friction contact would steadily increase or decrease depending on the sign of the excitation offset F_0. In practical situations the relative displacement is bounded, which ultimately results in a restricted damper efficiency. Additionally, the serial arrangement of a spring and friction element is represented for case where the third spring tends to zero ($c_3 \to 0$). With an adequate choice of the breakaway friction force the proposed dampers are able to limit amplitudes, despite the dissipation being only proportional to the displacement amplitude. These dampers are able to limit the amplitudes of the main mass, while maintaining the advantage of an antiresonant frequency. Additionally, depending on the main objective, either the dynamic vibration absorber or the dynamic vibration isolator can be chosen to reduce the amplitudes in the second eigenfrequency or in both eigenfrequencies respectively. However, the dynamic vibration absorber has the additional advantage that it is an add-on solution and can thus be added to existing systems. Apart from the practical advantages, the dynamics of both system are investigated. Using the linear system an estimation for the breakaway amplitude is obtained. This estimate allows a description of the systems dynamics outside the resonance regimes. For the dynamic vibration absorber a condition for the existence of an antiresonant frequency is derived, whereas for the dynamic vibration isolator this frequency is always present. A numerical model based on a Karnopp-friction contact is presented and used to study the influence of the newly introduced system parameters. Examining the equations of motion of the system with the nonlinear modal decoupling and averaging methods leads to implicit functions for the frequency-response curves. The analysis of these functions results in characteristic values of the damper's dynamics e.g. maximal amplitude and optimal friction values. Lastly, the analytical results are validated by the comparison with the numerical model.

The parameter studies in Sections 3.2 and 3.3 show a greater amplitude reduction with lower stiffness values of the partly operational spring c_3. This case is not analytically investigated in this work, since these values of c_3 lie outside the valid parameter range for the chosen method. For the same reason high values of $\boldsymbol{R}$ are not investigated. However, this is not critical, since the optimal friction value lies within the method's valid parameter range. In order to fully describe amplitude reduction potential of both dampers, an analytical solution for low stiffness values is required. The numerical and analytical models in this work use a simple friction model with identical values for the sticking and slipping friction forces, which can be further improved.

The damper limitations are apparent, when the excitation force on the dampers varies. As seen in the parameter studies in Section 3, when the friction force is not properly tuned to the excitation force large vibration amplitudes are observed for both dampers. As such if the magnitude of the excitation force changes the previous optimal force becomes inadequate and unable to quench unwanted oscillations. For this cases a semi-active or active control should prove advantageous.

Regarding the practical implementation of such dampers the design of springs parallel to friction elements is common in automotive clutches. A practical implementation is possible both dampers in order to reduce torsional vibrations in drive trains or translational vibrations in general. The implementation against torsional vibrations can be implemented using existing technology of clutches and clutch actuators, whereas for the translational motions special design is required. A demonstrator of the designed principle is under development.

ACKNOWLEDGMENTS

This work has been supported by the DFG German Research Foundation Grant FI 1761/2-1 within the Priority Program SPP 1897 "Calm, Smooth and Smart - Novel Approaches for Influencing Vibrations by Means of Deliberately Introduced Dissipation".

CONFLICT OF INTEREST

The authors declare no potential conflict of interests.

REFERENCES

[1] J. C. Dixon, *The Shock Absorber Handbook*, John Wiley & Sons **2008**.
[2] M.-J. Yan, E. H. Dowell, Governing equations for vibrating constrained-layer damping sandwich plates and beams, *J. Appl. Mech.* **1972**, *39*, 1041.
[3] V. I. Babitsky, *Theory of Vibro-Impact Systems and Applications*, Springer Science & Business Media **2013**.
[4] Y. V. Mikhlin, S. N. Reshetnikova, Dynamical interaction of an elastic system and a vibro-impact absorber, *Mathematical Problems in Engineering* **2006**, *2006*.
[5] C. N. Bapat, S. Sankar, Multiunit impact damper – re-examined, *J. Sound Vib.* **1985**, *103*, 457.
[6] G. Luo, L. Ma, X. Lv, Dynamic analysis and suppressing chaotic impacts of a two-degree-of-freedom oscillator with a clearance, *Nonlinear Analysis: Real World Applications* **2009**, *10*, 756.
[7] S. F. Masri, General motion of impact dampers, *J. Acoust. Soc. Am.* **1970**, *47*, 229.

[8] A. Hartung, U. Retze, H.-P. Hackenberg, Impulse mistuning of blades and vanes, *J. Eng. Gas Turbines Power* **2017**, *139*, 072502.

[9] V. J. Modi, S. R. Munshi, An efficient liquid sloshing damper for vibration control, *Journal of Fluids and Structures* **1998**, *12*, 1055.

[10] J. S. Love, M. J. Tait, Multiple tuned liquid dampers for efficient and robust structural control, *Journal of Structural Engineering* **2015**, *141*, 04015045.

[11] M. Farid, O. V. Gendelman, Response regimes in equivalent mechanical model of strongly nonlinear liquid sloshing, *Int. J. Non-Linear Mech.* **2017**, *94*, 146.

[12] D. Tang, H. P. Gavin, E. H. Dowell, Study of airfoil gust response alleviation using an electro-magnetic dry friction damper. Part 1: Theory, *J. Sound Vib.* **2004**, *269*, 853.

[13] D. Tang, H. P. Gavin, E. H. Dowell, Study of airfoil gust response alleviation using an electro-magnetic dry friction damper. part 2: experiment, *J. Sound Vib.* **2004**, *269*, 875.

[14] S. J. Dyke, B. F. Spencer Jr, M. K. Sain, J. D. Carlson, An experimental study of MR dampers for seismic protection, *Smart Mater. Struct.* **1998**, *7*, 693.

[15] C. Greiner-Petter, A. S. Tan, T. Sattel, A semi-active magnetorheological fluid mechanism with variable stiffness and damping, *Smart Mater. Struct.* **2014**, *23*, 115008.

[16] Y. Starosvetsky, O. V. Gendelman, Vibration absorption in systems with a nonlinear energy sink: Nonlinear damping, *J. Sound Vib.* **2009**, *324*, 916.

[17] H. Jo, H. Yabuno, Amplitude reduction of parametric resonance by dynamic vibration absorber based on quadratic nonlinear coupling, *J. Sound Vib.* **2010**, *329*, 2205.

[18] F. Rüdinger, Optimal vibration absorber with nonlinear viscous power law damping and white noise excitation, *Journal of Engineering Mechanics* **2006**, *132*, 46–53.

[19] A. Lupini, M. Mitra, B. I. Epureanu, Application of tuned vibration absorber concept to blisk ring dampers: A nonlinear study, *J. Eng. Gas Turbines Power*.

[20] M. Mitra, A. Lupini, Bogdan I. Epureanu, pp. GT2019.

[21] G. Habiba, T. Detroux, G. Kerschen, in *MATEC Web of Conferences*, EDP Sciences **2014**, p. 01005.

[22] T. Detroux, G. Habib, L. Masset, G. Kerschen, Performance, robustness and sensitivity analysis of the nonlinear tuned vibration absorber, *Mech. Syst. Signal Process.* **2015**, *60*, 799.

[23] R. Viguié, G. Kerschen, On the functional form of a nonlinear vibration absorber, *J. Sound Vib.* **2010**, *329*, 5225.

[24] G. Habib, G. Kerschen, A principle of similarity for nonlinear vibration absorbers, *Physica D: Nonlinear Phenomena* **2016**, *332*, 1.

[25] E. P. Petrov, D. J. Ewins, Effects of mistuning on the forced response of bladed discs with friction dampers, *Imperial Coll of Science and Technology London (United Kingdom) Dept of Mechanical Engineering*, **2005**.

[26] E. Ciğeroğlu, H. N., Özgüven, Nonlinear vibration analysis of bladed disks with dry friction dampers, *J. Sound Vib.* **2006**, *295*, 1028.

[27] J. H. Wang, W. L. Shieh, The influence of a variable friction coefficient on the dynamic behavior of a blade with a friction damper, *J. Sound Vib.* **1991**, *149*, 137.

[28] M. Berthillier, C. Dupont, R. Mondal, J. J. Barrau, Blades forced response analysis with friction dampers, *J. Vib. Acoust.* **1998**, *120*, 468.

[29] E. H. Dowell, H. B. Schwartz, Forced response of a cantilever beam with a dry friction damper attached, part I: theory, *J. Sound Vib.* **1983**, *91*, 255.

[30] E. H. Dowell, H. B. Schwartz, Forced response of a cantilever beam with a dry friction damper attached, Part II: Experiment, *J. Sound Vib.* **1983**, *91*, 269.

[31] M. Krack, L. A. Bergman, A. F. Vakakis, On the efficacy of friction damping in the presence of nonlinear modal interactions, *J. Sound Vib.* **2016**, *370*, 209.

[32] F. Weber, J. Høgsberg, S. Krenk, Optimal tuning of amplitude proportional Coulomb friction damper for maximum cable damping, *Journal of Structural Engineering* **2010**, *136*, 123.

[33] B. Morgen, Y. Kurama, A friction damper for post-tensioned precast concrete beam-to-column joints, *PCI J* **2004**, *49*, 112.

[34] F. Ricciardelli, B. J. Vickery, Tuned vibration absorbers with dry friction damping, *Earthq. Eng. Struct. Dyn.* **1999**, *28*, 707.

[35] A. Fidlin, M. Lobos, On the limiting of vibration amplitudes by a sequential friction-spring element, *J. Sound Vib.* **2014**, *333*, 5970.

[36] N. Gafur, Untersuchung der dynamischen Wirkung eines reibungsbasierten Tilgers mittels der Mittelwertbildung, Master's thesis, Karlsruhe Institute of Technology **2017**.

[37] R. I. Leine, H. Nijmeijer, *Dynamics and Bifurcations of Non-Smooth Mechanical Systems*, vol. 18, Springer Science & Business Media **2013**.

[38] J. Voldřich, Modelling of the three-dimensional friction contact of vibrating elastic bodies with rough surfaces.

[39] A. Fidlin, *Nonlinear Oscillations in Mechanical Engineering*, Springer Science & Business Media **2005**.

[40] D. Karnopp, Computer simulation of stick-slip friction in mechanical dynamic systems, *Journal of Dynamic Systems, Measurement, and Control* **1985**, *107*, 100.

[41] B. Marx, W. Vogt, *Dynamische Systeme: Theorie und Numerik*, Springer-Verlag **2010**.

[42] B. D. Yang, M. L. Chu, C. H. Menq, Stick–slip–separation analysis and non-linear stiffness and damping characterization of friction contacts having variable normal load, *J. Sound Vib.* **1998**, *210*, 461.

[43] J. P. Den Hartog, *Mechanical Vibrations*, Courier Corporation **1985**.

[44] A. Fidlin, N. Gafur, *On the Dynamics of Friction Based Tuned Mass Dampers*, Proceedings of ENOC 2017, 9th EUROMECH Nonlinear Dynamics Conference **2017**.

How to cite this article: J. Aramendiz, A. Fidlin, K. Lei. Investigations on amplitude adaptive sequential friction-spring dampers. *Z Angew Math Mech*. 2021;101:e201800293. https://doi.org/10.1002/zamm.201800293

APPENDIX A: NONLINEAR RANGE ESTIMATION FOR THE VIBRATION ABSORBER AND VIBRATION ISOLATOR

This appendix addresses the estimation of the linear ranges of both dampers. Since the dampers are linear while in the stick-phase, their solution is easily obtained. At the limit amplitude $A_L(\Omega)$ the stiction condition is broken, and the system transitions into the nonlinear stick-slip range. The limit amplitude is estimated by introducing the linear solution into the stiction condition inequalities. The procedure is explained for the dynamic vibration absorber and afterwards summarized by for the dynamic vibration isolator.

The solution of the dynamic vibration absorber is obtained for the stick-phase via linear methods. Therefore the motion of the coordinates as well as the stiction force is known. Since in practical applications the homogeneous solution steadily decays only the forced response of the system is considered. The coordinates x_1, x_2, and u are given as

$$x_1(t) = \frac{(c_2 - m_2\Omega^2)F\sin\Omega t}{m_1 m_2\Omega^4 - (c_1 m_2 + (m_1+m_2)c_2)\Omega^2 + c_1 c_2} = A_1(\Omega)\sin\Omega t, \tag{A.1}$$

$$x_2(t) = \frac{c_2 F\sin\Omega t}{m_1 m_2\Omega^4 - (c_1 m_2 + (m_1+m_2)c_2)\Omega^2 + c_1 c_2} = \frac{A_1(\Omega)c_2}{c_2 - m_2\Omega^2}\sin\Omega t, \tag{A.2}$$

$$u(t) = x_2(t) - w_0 \quad \& \quad w_0 = const. \tag{A.3}$$

Introducing Equations (A.1)–(A.3) in the stiction force and the stiction condition yields

$$|H(t)| = |c_2(u(t) - x_1(t)) - c_3(x_2(t) - u(t))| = |c_2(x_2(t) - w_0 - x_1(t)) - c_3 w_0| \le R, \tag{A.4}$$

$$= \left|\left(\frac{c_2^2}{c_2 - m_2\Omega^2} - c_2\right)A_1(\Omega)\sin\Omega t - (c_2+c_3)w_0\right| = \left|\frac{m_2\Omega^2 c_2}{c_2 - m_2\Omega^2}A_1(\Omega)\sin\Omega t - (c_2+c_3)w_0\right| \le R. \tag{A.5}$$

Applying the triangle inequality on Equation (A.5) an estimate for the maximum value of the stiction for is obtained as

$$|H(t)| = \left|\frac{m_2\Omega^2 c_2}{c_2 - m_2\Omega^2}A_1(\Omega)\sin\Omega t - (c_2+c_3)w_0\right| \tag{A.6}$$

$$|H(t)| \le \left|\frac{m_2\Omega^2 c_2}{c_2 - m_2\Omega^2}A_1(\Omega)\sin\Omega t\right| + \left|-(c_2+c_3)w_0\right| \le \left|\frac{m_2\Omega^2 c_2}{c_2 - m_2\Omega^2}\right|A_1(\Omega) + (c_2+c_3)|w_0| \le R \tag{A.7}$$

Since the triangle inequality was applied Equation (A.7) represents a conservative estimate for the stiction force. Thus the motion fulling Equation (A.7) will surely be linear. An estimation of the frequency dependent limit amplitude of the linear system $A_L(\Omega)$ is obtained by considering the limit case of Equation (A.7). Oscillation amplitudes below $A_L(\Omega)$ lead to a system which is exclusively in the stick-phase, whereas amplitudes above $A_L(\Omega)$ lead to a system in the nonlinear range with alternating stick- and slip-phases. The limit amplitude is given as

$$A_1(\Omega) \le A_L(\Omega) = \left|\frac{m_2\Omega^2 - c_2}{m_2\Omega^2 c_2}\right|(R - (c_2+c_3)|w_0|), \quad \text{with } |w_0| \le \frac{R}{c_2+c_3}. \tag{A.8}$$

For the dynamic vibration isolator the solution of the stick-phase is identical to Equations (A.1)–(A.3) and is introduced into the stiction condition

$$|H| = |c_1 x_1 - (c_1+c_2)u_0| \le R. \tag{A.9}$$

An analogous procedure is used to determine the limit amplitude of the dynamic vibration isolator. The equations are summarized as follows

$$|H| = |c_1 A_1(\Omega)\sin\Omega t - (c_1 + c_3)u_0| \leq |c_1 A_1(\Omega)\sin\Omega t| + |-(c_1 + c_3)u_0|$$

$$|H| \leq |c_1 A_1(\Omega)| + |(c_1 + c_3)u_0| \leq R$$

$$A_1(\Omega) \leq A_L = \frac{R - (c_1 + c_3)|u_0|}{c_1}, \quad \text{with } |u_0| \leq \frac{R}{c_1 + c_3}.$$

APPENDIX B: PARAMETER STUDY RESULTS FOR THE COORDINATE x_2

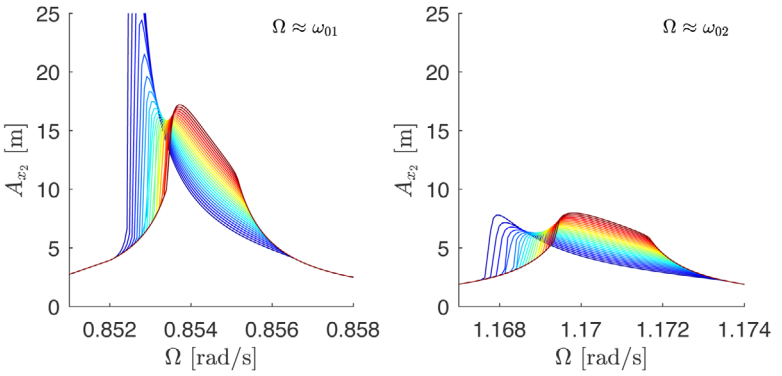

FIGURE B1 Parameter study: dynamic vibration absorber - breakaway force $R \in [0.3\text{N(blue)}, 0.8\text{N(red)}]$ in steps of 0.02 N. With $m_1 = 1\text{kg}$, $m_2 = 0.1\text{kg}$, $c_1 = 1\text{N/m}$, $c_2 = 0.1\text{N/m}$, $c_3 = 10\text{N/m}$, $F = 0.01\text{N}$

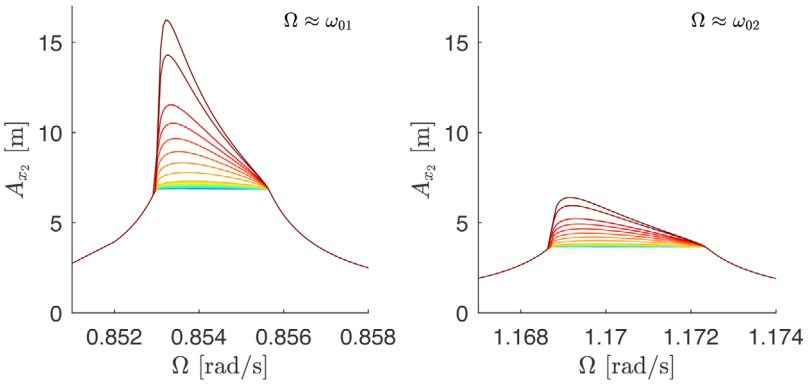

FIGURE B2 Parameter study: dynamic vibration absorber - stiffness $c_3 \in [0.01\text{N/m(blue)}, 10\text{N/m(red)}]$ in steps of 0.01 N/m until 1 N/m afterwards in steps of 1N/m. With $m_1 = 1\text{kg}$, $m_2 = 0.1\text{kg}$, $c_1 = 1\text{N/m}$, $c_2 = 0.1\text{N/m}$, $R = 0.5\text{N}$, $F = 0.01\text{N}$

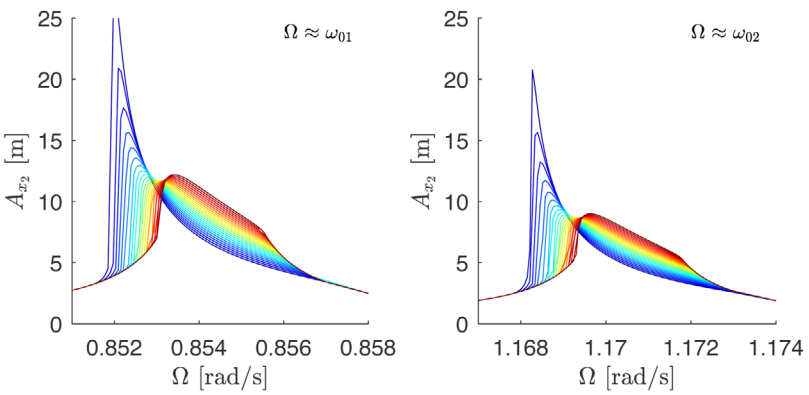

FIGURE B3 Parameter study: dynamic vibration isolator - breakaway force $R \in [0.9\text{N(blue)}, 2.0\text{N(red)}]$ in steps of 0.05 N. With $m_1 = 1\text{kg}$, $m_2 = 0.1\text{kg}$, $c_1 = 1\text{N/m}$, $c_2 = 0.1\text{N/m}$, $c_3 = 100\text{N/m}$, $F = 0.01\text{N}$

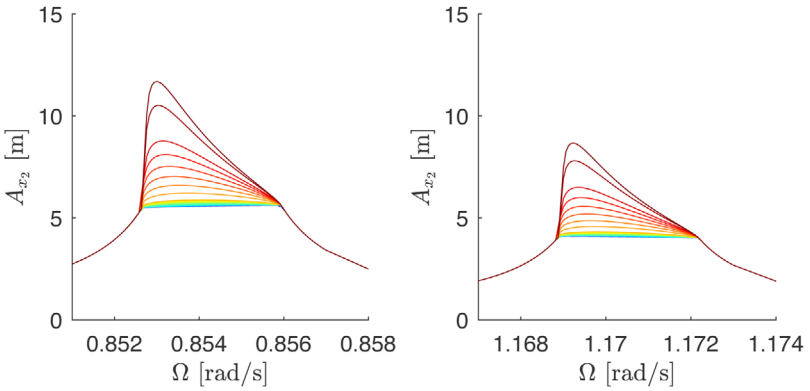

FIGURE B4 Parameter study: dynamic vibration isolator - stiffness $c_3 \in [0.1\text{N/m(blue)}, 100\text{N/m(red)}]$ in steps of 0.1 N/m until 1, afterwards steps of 1 N/m until 10 N/m, and finally steps of 10 N/m until 100 N/m. With $m_1 = 1\text{kg},\ m_2 = 0.1\text{kg},\ c_1 = 1\text{N/m},\ c_2 = 0.1\text{N/m},\ R = 1.5\text{N},\ F = 0.01\text{N}$

APPENDIX C: LINEAR ESTIMATE OF THE MODAL DECOUPLING VALIDITY

First, it is assumed that the frequency response curves of the modal coordinates have the form

$$q_i \sim \frac{\varepsilon f}{|\eta^2 - \eta_i^2|}. \tag{C.1}$$

Without loss of generality the first coordinate is considered; it applies that $q_1 = \mathcal{O}(1)$ when the $|\eta - \eta_1| = \mathcal{O}(\varepsilon)$ or in other words when $\eta = \eta_1 + \mathcal{O}(\varepsilon)$. That said, the magnitude of the second modal coordinate is investigated in the vicinity of the first eigenfrequency. It follows that

$$\eta = \eta_1 + \mathcal{O}(\varepsilon) \rightarrow q_2 = \frac{\varepsilon f}{|\eta_1^2 - \eta_2^2|} + \mathcal{O}(\varepsilon). \tag{C.2}$$

In order for $q_2 = \mathcal{O}(\varepsilon)$ the following relation must apply

$$\eta_1 - \eta_2 = \mathcal{O}(1). \tag{C.3}$$

APPENDIX D: FIRST ORDER AVERAGING EQUATIONS FOR THE DYNAMIC VIBRATION ISOLATOR

The Van-der-Pol transformations are the same as for the dynamic vibration absorber:

$$\begin{aligned} q_1 &= A_1 \sin\varphi_1, \quad \dot{\varphi}_1 = A_1\eta_1 \cos\varphi_1 \\ q_2 &= A_2 \sin\varphi_2, \quad \dot{\varphi}_2 = A_2\eta_2 \cos\varphi_2. \end{aligned} \tag{D.1}$$

The transformation above leads to the system in standard for for both modal coordinates

$$\begin{aligned} A_1' &= \frac{r_{11}}{\eta_1} w(q_1)\cos\varphi_1 - \varepsilon\frac{r_{11}}{\eta_1} f \sin(\psi_1 - \varphi_1)\cos\varphi_1 \\ \psi_1' &= \varepsilon\delta_1 - \frac{r_{11}}{A_1\eta_1} w(q_1)\cos\varphi_1 + \varepsilon\frac{r_{11}}{A_1\eta_1} f \sin(\psi_1 - \varphi_1)\cos\varphi_1 \\ \varphi_1' &= \eta_1 - \frac{r_{11}}{A_1\eta_1} w(q_1)\cos\varphi_1 + \varepsilon\frac{r_{11}}{A_1\eta_1} f \sin(\psi_1 - \varphi_1)\cos\varphi_1 \end{aligned} \tag{D.2}$$

$$\begin{aligned} A_2' &= \frac{r_{12}}{\eta_2} w(q_2)\cos\varphi_2 - \varepsilon\frac{r_{12}}{\eta_2} f \sin(\psi_2 - \varphi_2)\cos\varphi_2 \\ \psi_2' &= \varepsilon\delta_2 - \frac{r_{12}}{A_2\eta_2} w(q_2)\cos\varphi_2 + \varepsilon\frac{r_{12}}{A_2\eta_2} f \sin(\psi_2 - \varphi_2)\cos\varphi_2 \\ \varphi_2' &= \eta_2 - \frac{r_{12}}{A_2\eta_2} w(q_2)\cos\varphi_2 + \varepsilon\frac{r_{12}}{A_2\eta_2} f \sin(\psi_2 - \varphi_2)\cos\varphi_2. \end{aligned} \tag{D.3}$$

The averaging of Equations (D.2) and (D.3) yields

$$\bar{A}_1' = \left\langle A_1' \right\rangle_{\varphi_1} = \frac{\varepsilon}{\eta_1}\left(\zeta_{w_1,\cos} - \frac{r_{11}}{2\eta_1} f \sin\psi_1\right)$$

$$\bar{\psi}_1' = \left\langle \psi_1' \right\rangle_{\varphi_1} = \frac{\varepsilon}{\eta_1}\left(\delta_1 + \zeta_{w_1,\sin} - \frac{r_{11}}{2\eta_1 A_1} f \cos\psi_1\right) \tag{D.4}$$

$$\bar{A}_2' = \left\langle A_2' \right\rangle_{\varphi_2} = \frac{\varepsilon}{\eta_2}\left(\zeta_{w_2,\cos} - \frac{r_{12}}{2\eta_2} f \sin\psi_2\right)$$

$$\bar{\psi}_2' = \left\langle \psi_2' \right\rangle_{\varphi_2} = \frac{\varepsilon}{\eta_2}\left(\delta_2 + \zeta_{w_2,\sin} - \frac{r_{12}}{2\eta_2 A_2} f \cos\psi_2\right) \tag{D.5}$$

with

$$\zeta_{w_1,\cos} = -\frac{2\rho\left(\kappa r_{11}\bar{A}_1 - \rho\right)}{\kappa \bar{A}_1 \eta_1 \pi}$$

$$\zeta_{w_1,\sin} = -\frac{1}{4\kappa \bar{A}_1^2 \pi \eta_1}\left(\kappa^2 r_{11}^2 \bar{A}_1^2\left(\pi + 2\arcsin\left(\frac{\kappa r_{11}\bar{A}_1 - 2\rho}{\kappa r_{11}\bar{A}_1}\right)\right) + (4\kappa r_{11}\,\bar{A}_1 - 8\rho)\sqrt{\rho(\kappa r_{11}\,\bar{A}_1 - \rho)}\right), \tag{D.6}$$

$$\zeta_{w_2,\cos} = -\frac{2\rho\left(\kappa r_{12}\bar{A}_2 - \rho\right)}{\kappa \bar{A}_2 \eta_2 \pi}$$

$$\zeta_{w_2,\sin} = -\frac{2}{4\kappa \bar{A}_2^2 \pi \eta_2}\left(\kappa^2 r_{12}^2 \bar{A}_2^2\left(\pi + 2\arcsin\left(\frac{\kappa r_{12}\bar{A}_2 - 2\rho}{\kappa r_{12}\bar{A}_2}\right)\right) + (4\kappa r_{12}\,\bar{A}_2 - 8\rho)\sqrt{\rho(\kappa r_{12}\,\bar{A}_2 - \rho)}\right). \tag{D.7}$$

Calculating the stationary solution ($\bar{A}_1' = \bar{\psi}_1' = \bar{A}_2' = \bar{\psi}_2' = 0$) for Equation (D.6) and (D.7) results in the implicit frequency-response functions

$$\eta = \eta_1 + \varepsilon\zeta_{w_1,\sin} \pm \frac{\varepsilon}{2\bar{A}_1\eta_1}\sqrt{r_{11}^2 f^2 - 4\zeta_{w_1,\cos}^2 \eta_1^2}, \tag{D.8}$$

$$\eta = \eta_2 + \varepsilon\zeta_{w_2,\sin} \pm \frac{\varepsilon}{2\bar{A}_2\eta_2}\sqrt{r_{12}^2 f^2 - 4\zeta_{w_2,\cos}^2 \eta_2^2}. \tag{D.9}$$

By analyzing Equation (D.8) and (D.9) characteristic values of the damper are derived

$$\bar{A}_{1,\min 1} = \frac{\rho}{\kappa r_{11}}, \tag{D.10}$$

$$\bar{A}_{1,\min 2} = \frac{4\rho^2}{\kappa r_{11}\left(4r_{11}\rho - \pi f\right)}, \tag{D.11}$$

$$\bar{A}_{1,\max} = \frac{4\rho^2}{\kappa r_{11}\left(4r_{11}\rho + \pi f\right)}, \tag{D.12}$$

$$\bar{A}_{1,\min} = \max(\bar{A}_{2,\min 1}, \bar{A}_{2,\min 2}), \tag{D.13}$$

$$\rho_{1,\min} = \frac{\pi f}{4}, \tag{D.14}$$

$$\rho_{1,\text{opt}} = \frac{\pi f}{2}, \tag{D.15}$$

$$\bar{A}_{2,\min 1} = \frac{\rho}{\kappa r_{12}}, \tag{D.16}$$

$$\bar{A}_{2,\min 2} = \frac{4\rho^2}{\kappa r_{12}\left(4r_{12}\rho - \pi f\right)}, \tag{D.17}$$

$$\bar{A}_{2,\max} = \frac{4\rho^2}{\kappa r_{12}\left(4r_{12}\rho + \pi f\right)}, \tag{D.18}$$

$$\bar{A}_{2,\min} = \max(\bar{A}_{2,\min 1}, \bar{A}_{2,\min 2}), \tag{D.19}$$

$$\rho_{2,\min} = \frac{\pi f}{4}, \tag{D.20}$$

$$\rho_{2,\text{opt}} = \frac{\pi f}{2}. \tag{D.21}$$

In order to describe the original variables x_1 and x_2 the following transformations are applied

$$\eta \approx \eta_1 \;\Rightarrow\; \begin{cases} A_{x_1} \approx \bar{A}_1 |r_{11}| \\ A_{x_2} \approx \bar{A}_1 |r_{21}| \end{cases}, \tag{D.22}$$

$$\eta \approx \eta_2 \;\Rightarrow\; \begin{cases} A_{x_1} \approx \bar{A}_2 |r_{12}| \\ A_{x_2} \approx \bar{A}_2 |r_{22}| \end{cases}. \tag{D.23}$$